Available online at www.synsint.com

Synthesis and Sintering

ISSN 2564-0186 (Print), **ISSN** 2564-0194 (Online)

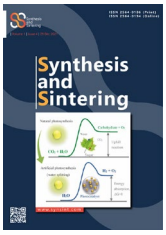

Role of Ti_3AlC_2 MAX phase on characteristics of in-situ synthesized TiAl intermetallics. Part II: phase evolution

Maryam Akhlaghi [a], Esmaeil Salahi [b,*], Seyed Ali Tayebifard [a], Gert Schmidt [c]

[a] *Semiconductors Department, Materials and Energy Research Center (MERC), Karaj, Iran*
[b] *Ceramics Department, Materials and Energy Research Center (MERC), Karaj, Iran*
[c] *Faculty of Mechanical, Process and Energy Engineering, TU Bergakademie, Freiberg, Germany*

A B S T R A C T

In this research, the 2nd part of a series of papers on the processing and characterization of TiAl–Ti_3AlC_2 composites, the phase evolution during the manufacturing process was investigated by X-ray diffraction (XRD) analysis and Rietveld refinement method. Metallic Ti and Al powders with different amounts of previously-synthesized Ti_3AlC_2 additives (10, 15, 20, 25 and 30 wt%) were ball-milled and densified by spark plasma sintering (SPS) under 40 MPa for 7 min at 900 °C. Before the sintering process, XRD test verified that the powder mixtures contained metallic Ti and Al as well as Ti_3AlC_2 and TiC (lateral phase synthesized with Ti_3AlC_2) phases. In the sintered composites, the in-situ synthesis of TiAl and Ti_3Al intermetallics as well as the presence of Ti_3AlC_2 and the formation and Ti_2AlC MAX phases were disclosed. The weight percentage of each phase in the final composition of the samples and the crystallite size of different phases were calculated by the Rietveld refinement method based on the XRD patterns. The size of Ti_3AlC_2 crystallites in sintered samples was compared with the crystallite size of synthesized Ti_3AlC_2 powder.

KEYWORDS

Spark plasma sintering
TiAl
Ti_3AlC_2
Phase analysis
Rietveld refinement
Crystallite

1. Introduction

TiAl-based composites have gained researcher's attentions because of their unique characteristics including low density, high melting point, as well as excellent corrosion properties, good creep and oxidation resistance [1–6]. However, low-temperature ductility and weak formability of TiAl matrix materials have led to limitation of their application and development [7–10]. Different tricks such as choosing appropriate manufacturing method and addition of reinforcements have been used to dominate such shortcomings [11–13]. Spark plasma sintering is a recently developed method employing for fabrication of various ceramics, polymers, and metals [14–17]. Reproducibility, high sintering rate, and lower consolidation temperatures are the advantages of this method, in comparison to traditional sintering techniques that make easy to attain finer and homogeneous microstructures [18–23].

Some metal additives like Co and Fe improved the ductility of TiAl through the occupation of Al sites by these atoms. In contrast, Ni addition to TiAl resulted in ductility degradation owing to the formation of NiTi phase at the grain boundaries [24]. Protective surface layer formation of Al_2O_3 as a result of adding Nb or Ta to TiAl matrix improved oxidation resistance at high temperatures [25]. TiAl intermetallic with low wear and high lubricity was fabricated by using Cu-coated graphite. Soft tribo-layer formation and in-situ synthesis of TiC with high inherent hardness are the reasons of such excellent tribological feature [26]. Improvement in the elevated-temperature ductility and room-temperature strength of TiAl material was attributed to the formation of laths due to the addition of Sn [27]. It is reported that Ru has an effective impact on both ductility and strength of TiAl materials through grain refinement mechanism [28].

* Corresponding author. *E-mail address:* e-salahi@merc.ac.ir (E. Salahi)
Received 27 September 2021; Received in revised form 26 December 2021; Accepted 26 December 2021.

https://doi.org/10.53063/synsint.2021.1453

In addition to metals, using the ceramic compounds is a beneficial way to reinforce the TiAl-based composites. The manufacturing of Ti_5Si_3 reinforced TiAl intermetallic by combustion synthesis and hot pressing led to the in-situ formation of Ti_5Si_3 that enhanced strength and ductility. Compression strength of hot pressed TiAl materials was significantly improved by nano-sized TiB_2 addition [29]. It is also reported that TiAl-based composite with increased density and improved mechanical performance can be fabricated via TiB_2 reinforcing, which formed by self-propagating high-temperature synthesis technique [30]. Using high amount of Y_2O_3 additive in spark plasma sintered TiAl material resulted in boosted properties via the formation and dispersion of strip-like YAl_2 precipitates [31]. Elongation and the ultimate tensile strength of high-Nb containing TiAl intermetallic increased by adding nano-Y_2O_3 via fine-grain strengthening [32].

Given that the density and coefficient of thermal expansion of the TiAl are close to those of MAX phases like Ti_2AlC with lamellar structure, these materials are used as additives in TiAl intermetallics [33]. Ti_2AlC reinforced TiAl were manufactured by powders of Ti, Al and carbon elements employing SHS method [34]. Vacuum arc melting process was utilized to synthesize TiAl–Ti_2AlC composites using graphite, Ti, and Al powders [35]. TiAl–Ti_2AlC composite materials with layered structure were in-situ synthesized using Al, Ti and TiC powders as the raw materials by reactive hot-pressing process. It is reported that TiAl formed by reaction between Al and Ti below 900 ºC; and subsequently, TiC reacted with formed TiAl above 900 ºC. Increasing the Ti_2AlC content gradually enhanced the density and hardness [36]. A mechanically alloyed Ti–Al powder mixture with CNTs was utilized for in-situ formation of TiAl–Ti_2AlC composite with high density and refined microstructure including a continuous interpenetrating network of Ti_2AlC by spark plasma sintering [37]. Ti, Al and Ti_3AlC_2 powders as the initial compounds were used to fabricate TiAl–Ti_3AlC_2 sample by spark plasma sintering at temperature of 1000 °C under 40 MPa for 15 min [38].

In this work, in-situ formed TiAl matrix composites with 10, 15, 20, 25 and 30 wt% Ti_3AlC_2 additives were manufactured by SPS technology under 40 MPa for 7 min at 900 °C. Phase evolution of TiAl–Ti_3AlC_2 composites during the spark plasma synthesis and sintering is investigated in this paper as the second part of a series of publications. The first part of this series of papers, which has been recently published (Ref. [39]), was dedicated to sintering and densification, and in the next parts, the microstructure, mechanical properties and fractographical characterizations of them will be studied.

2. Experimental procedure

Metallic titanium and aluminum powders with equal molar ratios were used as starting materials for in-situ fabrication of TiAl matrix. The technical specifications of the raw materials are reported in Ref. [39]. Ti_3AlC_2 MAX phase, which was previously synthesized in our laboratory through the mechanically-activated self-propagating high-temperature synthesis route (MASHS) [40], was used as the reinforcement material with different amounts of 10, 15, 20, 25 and 30 wt%.

Five powder mixtures of Ti, Al and Ti_3AlC_2 materials were ball-milled for 1 h at 300 rpm, and then filled into the graphite dies with internal diameters of 3 cm, which already had been lined with thin graphite foils. Phase characterization was carried out on the prepared powder mixtures using an X-ray diffractometer (Philips-PW3710: λ_{Cu}-K_α=0.15406 nm, 40 kV, 30 mA).

An initial pressure of ~8 MPa and a vacuum of 12-15 Pa were applied to the powder mixtures inside an SPS chamber (model: 20T-10). Then, the densification through spark plasma sintering process was performed at 900 °C for 7 min under 40 MPa. After grinding and cleaning, the sintered samples were polished with sandpaper from 100 to 5000 mesh and then with diamond paste. Subsequently, phase analyses were also performed on the prepared surface of the samples using an X-ray diffractometer.

3. Results and discussion

Fig. 1 shows the X-ray diffraction pattern of the powder mixture, after ball-milling and before sintering, used for the fabrication of TiAl-based composite reinforced with 20 wt% Ti_3AlC_2. As shown in this pattern, the powder mixture contains metallic Ti and Al phases as well as Ti_3AlC_2 and TiC compounds. The first three ones, the metallic and MAX phases, were added directly to the powder mixture, but the detection of the TiC was due to impurities along with the synthesized Ti_3AlC_2 phase. Our previous published report and calculations [40], using the Rietveld refinement method, showed that the purity of the Ti_3AlC_2 phase synthesized in our laboratory was 85 wt%, and therefore, the presence of about 15 wt% TiC in the MAX phase is cognizable.

The results of X-ray diffraction analyses after sintering of the samples at 900 °C are presented in Fig. 2. The final phases including TiAl, Ti_3Al, Ti_3AlC_2 and Ti_2AlC appeared in the fabricated composites. Reference JCPDS card numbers of 00-052-0875, 00-029-0095, 00-052-0859 and 03-065-0428 were used for identification of Ti_3AlC_2, Ti_2AlC, Ti_3Al and TiAl phases, respectively. It seems that the primary metal components (titanium and aluminum) have been completely consumed during the sintering process and converted to the intermetallic compounds of TiAl and Ti_3Al. It is worth noting that in addition to the initial Ti_3AlC_2 MAX phase, a new MAX phase of Ti_2AlC has also been generated. Meanwhile, the lateral phase of TiC associated with the as-synthesized Ti_3AlC_2 phase that had been detected in the X-ray diffraction pattern of the as-milled powders (Fig. 1), was not found in

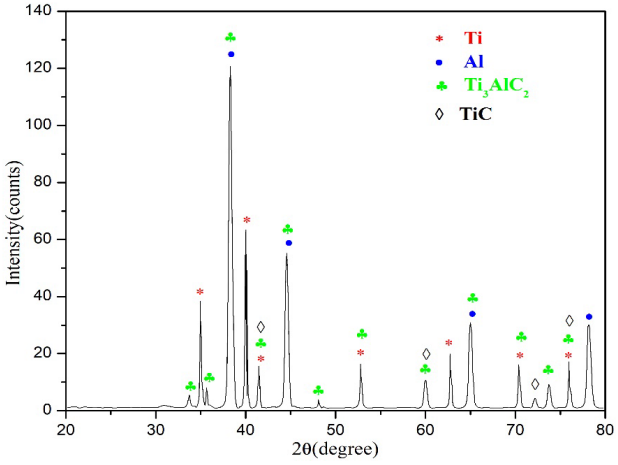

Fig. 1. X-ray diffraction pattern of the milled titanium, aluminum and Ti_3AlC_2 powders used for fabrication of the TiAl-20 wt% Ti_3AlC_2 composite.

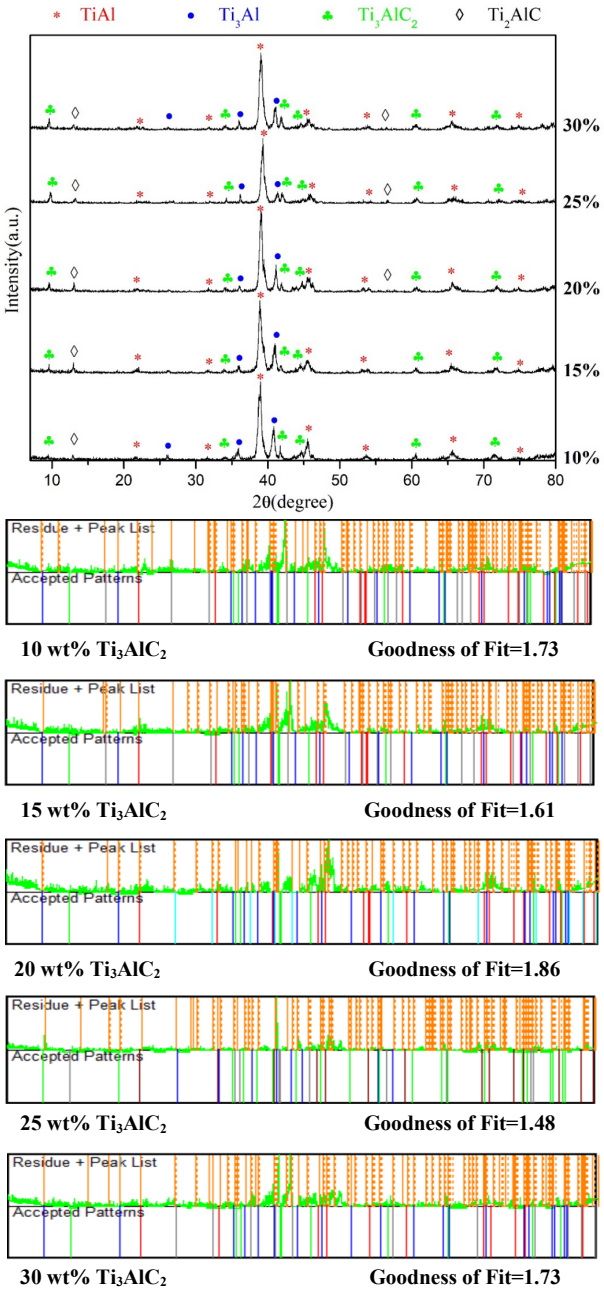

Fig. 2. X-ray diffraction patterns of the as-sintered TiAl-based composites reinforced with different amounts of Ti_3AlC_2 additives.

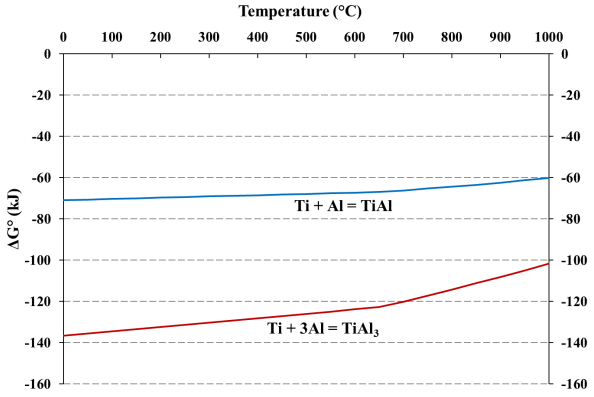

Fig. 3. Gibbs free energy changes of formation of two intermetallics between Ti and Al versus temperature.

the X-ray diffraction patterns (Fig. 2) of any of the sintered composite specimens, indicating complete TiC consumption during the manufacturing process.

Several intermetallic compounds can be obtained from the reaction of primary titanium and aluminum metal powders, including TiAl, $TiAl_3$ and Ti_3Al in accordance with Eqs. 1-3, respectively. In general, Gibbs free energy changes (ΔG°) predict the possibility of a reaction occurring spontaneously, and that reaction occurs when ΔG° is negative. Fig. 3 shows these changes for the formation reactions of TiAl and $TiAl_3$ intermetallic phases from 0 to 1000 °C using HSC Chemistry software. Unfortunately, Ti_3Al phase data was not available in the database of that software.

$$Ti + Al = TiAl \quad (1)$$

$$Ti + 3Al = TiAl_3 \quad (2)$$

$$3Ti + Al = Ti_3Al \quad (3)$$

As shown in Fig. 3, because the Gibbs free energy changes associated with Eq. 2 have negative values than Eq. 1 at all temperatures, the formation of the $TiAl_3$ phase is preferable to the TiAl phase. Ai et al. [41] also showed that the $TiAl_3$ phase is preferentially formed by the reaction of titanium with molten aluminum, which releases a lot of heat. Subsequently, with further increase in temperature, $TiAl_3$ reacts with Ti, and therefore, intermetallic phases of TiAl and Ti_3Al appear according to Eq. 4. Finally, part of the formed TiAl reacts with the lateral TiC phase, present in the previously -synthesized Ti_3AlC_2 powder, and the Ti_2AlC phase is synthesized based on Eq. 5.

Table 1. Quantitative phase analysis of the as-sintered composites using the Rietveld refinement method.

Sample no.	Ti_3AlC_2 content in initial mixture (wt%)	TiAl (wt%)	Ti_3Al (wt%)	Ti_3AlC_2 (wt%)	Ti_2AlC (wt%)
1	10	55.4	31.7	12.9	-
2	15	60.2	24.3	15.5	-
3	20	63.2	16.8	17.5	2.5
4	25	62.1	14.0	21.2	2.7
5	30	55.7	17.0	24.3	3.0

$$TiAl_3 + 4Ti = 2TiAl + Ti_3Al \quad (4)$$

$$TiAl + TiC = Ti_2AlC \quad (5)$$

The above analyzes and discussions, which are consistent with the thermodynamic predictions and the results of XRD analysis, indicate that it is possible to fabricate the TiAl–Ti_3Al-based composites reinforced with Ti_3AlC_2–Ti_2AlC MAX phases using Ti, Al and Ti_3AlC_2 as raw materials through SPS technology.

The results of quantitative analyzes, by Rietveld refinement method, to determine the percentage of matrix phases (TiAl and Ti_3Al) and MAX phase reinforcements (Ti_3AlC_2 and Ti_2AlC) in the sintered composites are reported in Table 1. The total weight percentages of Ti_3AlC_2 and Ti_2AlC MAX phases in the final composition of the sintered samples are approximately equal to the amounts of Ti_3AlC_2 MAX phase added to the initial powder mixtures. The reason for this equality can bediscussed that the amount of lateral phase of TiC (15 wt%) in synthesized Ti_3AlC_2 powder is approximately equal to the amount of Ti_2AlC MAX phase synthesized during the sintering. The slight differences in the initial and final values can be attributed to the inherent inaccuracy of the X-ray diffraction test, the Rietveld refinement method, and the use of software for calculations. However, the results are valid because such differences are negligible. Since the amounts of MAX phase additive in the first two samples, which contained 10 and 15 wt% of Ti_3AlC_2, were less than the other samples, and therefore, less lateral TiC phase was added to their initial powder mixtures, the Rietveld analysis failed to estimate the Ti_2AlC content. Although one of the diffraction peaks of Ti_2AlC phase is seen in the X-ray diffraction patterns of these samples (Fig. 2), but its quantitative identification was not possible for TiAl–(10,15) wt% Ti_3AlC_2 composites.

Table 2 presents the results of the crystallite size calculations of the TiAl, Ti_3Al and Ti_3AlC_2 phases using the XRD methodology. It is worth noting that the nature of this method is approximate and the measurement errors are inevitable. Due to the small size of crystallites, the title of nanocomposite can be applied to the SPSed samples in this research work. Comparing the size of Ti_3AlC_2 crystallites in the sintered samples (39-41 nm; as seen in Table 2) with the size of the synthesized Ti_3AlC_2 powder (39 nm; reported in Ref. [40]), a slight increase in crystallite size occurred during the SPS process. Such an observation, i.e. the minimal crystallite growth, can be related to the nature of spark plasma sintering, and the short dwell time applied in this manufacturing process.

Table 2. Determination of size of crystallites using the XRD analysis for the as-sintered composites.

Composite	TiAl (nm)	Ti_3Al (nm)	Ti_3AlC_2 (nm)
TiAl–10 wt% Ti_3AlC_2	14	17	41
TiAl–15 wt% Ti_3AlC_2	13	17	39
TiAl–20 wt% Ti_3AlC_2	16	11	39
TiAl–25 wt% Ti_3AlC_2	12	22	40
TiAl–30 wt% Ti_3AlC_2	12	22	40

4. Conclusions

In the 2nd part of a series of papers, dedicated to processing and characterization of TiAl–Ti_3AlC_2 composites, phase evolution during the SPS of ball-milled Ti, Al and Ti_3AlC_2 powders was studied. After the ball-milling process, in addition to the starting components of Ti, Al and Ti_3AlC_2, the lateral TiC (synthesized with Ti_3AlC_2) was also detected by XRD analysis. During the sintering process, TiAl and Ti_3Al intermetallics and Ti_2AlC MAX phase were in-situ synthesized and appeared in the final composition along with the initial Ti_3AlC_2 MAX phase. The $TiAl_3$ phase was initially formed by the reaction of Ti with molten Al. It then reacted with Ti to form TiAl and Ti_3Al. In addition, part of the TiAl reacted with the TiC to synthesize Ti_2AlC. The results of quantitative phase analysis by the Rietveld refinement method on different phases in sintered samples were in good agreement with the phase evolutions happened on the starting components in the powder mixtures. The results of crystallite size calculations, 39-41 nm for the sintered samples compared to 39 nm for the synthesized powder, showed that no significant growth in Ti_3AlC_2 crystallites occurred during the SPS process.

References

[1] M.R. Kabir, L. Chernova, M. Bartsch, Numerical investigation of room-temperature deformation behavior of a duplex type γTiAl alloy using a multi-scale modeling approach, Acta Mater. 58 (2010) 5834–5847. https://doi.org/10.1016/j.actamat.2010.06.058.

[2] Z. Duan, Y. Han, X. Song, H. Chen, Creep behaviour of equiaxed fine-grain γ-TiAl-based alloy prepared by powder metallurgy, Mater. Sci. Technol. 36 (2020) 1457–1464. https://doi.org/10.1080/02670836.2020.1790098.

[3] H. Huang, H. Ding, X. Xu, R. Chen, J. Guo, H. Fu, Phase transformation and microstructure evolution of a beta-solidified gamma-TiAl alloy, J. Alloys Compd. 860 (2021) 158082. https://doi.org/10.1016/j.jallcom.2020.158082.

[4] H.P. Lim, W.Y.H. Liew, G.J.H. Melvin, Z.-T. Jiang, A Short Review on the Phase Structures, Oxidation Kinetics, and Mechanical Properties of Complex Ti-Al Alloys, Materials (Basel). 14 (2021) 1677. https://doi.org/10.3390/ma14071677.

[5] Z. Trzaska, G. Bonnefont, G. Fantozzi, J.-P. Monchoux, Comparison of densification kinetics of a TiAl powder by spark plasma sintering and hot pressing, Acta Mater. 135 (2017) 1–13. https://doi.org/10.1016/j.actamat.2017.06.004.

[6] Y. Jiang, Y. He, H. Gao, Recent progress in porous intermetallics: Synthesis mechanism, pore structure, and material properties, J. Mater. Sci. Technol. 74 (2021) 89–104. https://doi.org/10.1016/j.jmst.2020.10.007.

[7] C.Y. Teng, N. Zhou, Y. Wang, D.S. Xu, A. Du, Y.H. Wen, R. Yang, Phase-field simulation of twin boundary fractions in fully lamellar TiAl alloys, Acta Mater. 60 (2012) 6372–6381. https://doi.org/10.1016/j.actamat.2012.08.016.

[8] G.H. Cao, A.M. Russell, C.-G. Oertel, W. Skrotzki, Microstructural evolution of TiAl-based alloys deformed by high-pressure torsion, Acta Mater. 98 (2015) 103–112. https://doi.org/10.1016/j.actamat.2015.07.012.

[9] Y. Garip, Investigation of isothermal oxidation performance of TiAl alloys sintered by different processing methods, Intermetallics. 127 (2020) 106985. https://doi.org/10.1016/j.intermet.2020.106985.

[10] J. Shen, L. Hu, L. Zhang, W. Liu, A. Fang, Y. Sun, Synthesis of TiAl/Nb composites with concurrently enhanced strength and plasticity by powder metallurgy, Mater. Sci. Eng. A. 795 (2020) 139997. https://doi.org/10.1016/j.msea.2020.139997.

[11] H.P. Qu, P. Li, S.Q. Zhang, A. Li, H.M. Wang, The effects of heat treatment on the microstructure and mechanical property of laser melting deposition γ-TiAl intermetallic alloys, Mater. Des. 31 (2010) 2201–2210. https://doi.org/10.1016/j.matdes.2009.10.045.
[12] H. Clemens, A. Bartels, S. Bystrzanowski, H. Chladil, H. Leitner, G. Dehm, R. Gerling, F.P. Schimansky, Grain refinement in γ-TiAl-based alloys by solid state phase transformations, Intermetallics. 14 (2006) 1380–1385. https://doi.org/10.1016/j.intermet.2005.11.015.
[13] L. Xiang, F. Wang, J. Zhu, X. Wang, Mechanical properties and microstructure of Al2O3/TiAl in situ composites doped with Cr2O3, Mater. Sci. Eng. A. 528 (2011) 3337–3341. https://doi.org/10.1016/j.msea.2011.01.006.
[14] M. Mansoor, M. Mansoor, M. Mansoor, Z. Er, F. Çinar Şahin, Ab-initio study of paramagnetic defects in Mn and Cr doped transparent polycrystalline Al2O3 ceramics, Synth. Sinter. 1 (2021) 135–142. https://doi.org/10.53063/synsint.2021.1340.
[15] B. Nayebi, M. Shahedi Asl, M. Akhlaghi, Z. Ahmadi, S.A. Tayebifard, E. Salahi, M. Shokouhimehr, M. Mohammadi, Spark plasma sintering of TiB2-based ceramics with Ti3AlC2, Ceram. Int. 47 (2021) 11929–11934. https://doi.org/10.1016/j.ceramint.2021.01.033.
[16] M. Shahedi Asl, B. Nayebi, M. Akhlaghi, Z. Ahmadi, S.A. Tayebifard, E. Salahi, M. Shokouhimehr, M. Mohammadi, A novel ZrB2-based composite manufactured with Ti3AlC2 additive, Ceram. Int. 47 (2021) 817–827. https://doi.org/10.1016/j.ceramint.2020.08.193.
[17] F. Sadegh Moghanlou, M. Vajdi, M. Sakkaki, S. Azizi, Effect of graphite die geometry on energy consumption during spark plasma sintering of zirconium diboride, Synth. Sinter. 1 (2021) 54–61. https://doi.org/10.53063/synsint.2021.117.
[18] M. Saravana Kumar, S. Rashia Begum, M. Vasumathi, C.C. Nguyen, Q. Van Le, Influence of molybdenum content on the microstructure of spark plasma sintered titanium alloys, Synth. Sinter. 1 (2021) 41–47. https://doi.org/10.53063/synsint.2021.1114.
[19] N.F. Mogale, W.R. Matizamhuka, Spark Plasma Sintering of Titanium Aluminides: A Progress Review on Processing, Structure-Property Relations, Alloy Development and Challenges, Metals (Basel). 10 (2020) 1080. https://doi.org/10.3390/met10081080.
[20]M. Musi, B. Galy, J.-P. Monchoux, A. Couret, H. Clemens, S. Mayer, In-situ observation of the phase evolution during an electromagnetic-assisted sintering experiment of an intermetallic γ-TiAl based alloy, Scr. Mater. 206 (2022) 114233. https://doi.org/10.1016/j.scriptamat.2021.114233.
[21] D. Wimler, J. Lindemann, T. Kremmer, H. Clemens, S. Mayer, Microstructure and mechanical properties of novel TiAl alloys tailored via phase and precipitate morphology, Intermetallics. 138 (2021) 107316. https://doi.org/10.1016/j.intermet.2021.107316.
[22] M. Vajdi, S. Mohammad Bagheri, F. Sadegh Moghanlou, A. Shams Khorrami, Numerical investigation of solar collectors as a potential source for sintering of ZrB2, Synth. Sinter. 1 (2021) 76–84. https://doi.org/10.53063/synsint.2021.128.
[23] M. Abdolahpour Salari, G. Merhan Muğlu, M. Rezaei, M. Saravana Kumar, H. Pulikkalparambil, S. Siengchin, In-situ synthesis of TiN and TiB2 compounds during reactive spark plasma sintering of BN–Ti composites, Synth. Sinter. 1 (2021) 48–53. https://doi.org/10.53063/synsint.2021.119.
[24] S. Shu, F. Qiu, C. Tong, X. Shan, Q. Jiang, Effects of Fe, Co and Ni elements on the ductility of TiAl alloy, J. Alloys Compd. 617 (2014) 302–305. https://doi.org/10.1016/j.jallcom.2014.07.199.
[25] P.V. Cobbinah, W. Matizamhuka, R. Machaka, M.B. Shongwe, Y. Yamabe-Mitarai, The effect of Ta additions on the oxidation resistance of SPS-produced TiAl alloys, Int. J. Adv. Manuf. Technol. 106 (2020) 3203–3215. https://doi.org/10.1007/s00170-019-04885-7.
[26] L. Wang, A.K. Tieu, Q. Zhu, J. Chen, J. Cheng, J. Yang, B. Kosasih, Achieving the excellent self-lubricity and low wear of TiAl intermetallics through the addition of copper coated graphite, Compos. Part B Eng. 198 (2020) 108223. https://doi.org/10.1016/j.compositesb.2020.108223.
[27] Q. Duan, Q. Luan, J. Liu, L. Peng, Microstructure and mechanical properties of directionally solidified high-Nb containing Ti–Al alloys, Mater. Des. 31 (2010) 3499–3503. https://doi.org/10.1016/j.matdes.2010.02.022.
[28] Q. Liu, P. Nash, The effect of Ruthenium addition on the microstructure and mechanical properties of TiAl alloys, Intermetallics. 19 (2011) 1282–1290. https://doi.org/10.1016/j.intermet.2011.04.005.
[29] S. Shu, B. Xing, F. Qiu, S. Jin, Q. Jiang, Comparative study of the compression properties of TiAl matrix composites reinforced with nano-TiB2 and nano-Ti5Si3 particles, Mater. Sci. Eng. A. 560 (2013) 596–600. https://doi.org/10.1016/j.msea.2012.10.001.
[30] C.L. Yeh, S.H. Su, In situ formation of TiAl–TiB2 composite by SHS, J. Alloys Compd. 407 (2006) 150–156. https://doi.org/10.1016/j.jallcom.2005.06.053.
[31] X. Gu, F. Cao, N. Liu, G. Zhang, D. Yang, H. Shen, D. Zhang, H. Song, J. Sun, Microstructural evolution and mechanical properties of a high yttrium containing TiAl based alloy densified by spark plasma sintering, J. Alloys Compd. 819 (2020) 153264. https://doi.org/10.1016/j.jallcom.2019.153264.
[32] Y. Guo, Y. Liang, J. Lin, F. Yang, Effect of Nano-Y2O3 Addition on Microstructure and Tensile Properties of High-Nb TiAl Alloy Prepared by Spark Plasma Sintering, Metals (Basel). 11 (2021) 1048. https://doi.org/10.3390/met11071048.
[33] X.H. Wang, Y.C. Zhou, Layered Machinable and Electrically Conductive Ti2AlC and Ti3AlC2 Ceramics: a Review, J. Mater. Sci. Technol. 26 (2010) 385–416. https://doi.org/10.1016/S1005-0302(10)60064-3.
[34] C.L. Yeh, Y.G. Shen, Formation of TiAl–Ti2AlC in situ composites by combustion synthesis, Intermetallics. 17 (2009) 169–173. https://doi.org/10.1016/j.intermet.2008.10.014.
[35] X.-J. Song, H.-Z. Cui, N. Hou, N. Wei, Y. Han, J. Tian, Q. Song, Lamellar structure and effect of Ti2AlC on properties of prepared in - situ TiAl matrix composites, Ceram. Int. 42 (2016) 13586–13592. https://doi.org/10.1016/j.ceramint.2016.05.152.
[36] C. Yang, F. Wang, T. Ai, J. Zhu, Microstructure and mechanical properties of in situ TiAl/Ti2AlC composites prepared by reactive hot pressing, Ceram. Int. 40 (2014) 8165–8171. https://doi.org/10.1016/j.ceramint.2014.01.012.
[37] F. Yang, F.T. Kong, Y.Y. Chen, S.L. Xiao, Effect of spark plasma sintering temperature on the microstructure and mechanical properties of a Ti2AlC/TiAl composite, J. Alloys Compd. 496 (2010) 462–466. https://doi.org/10.1016/j.jallcom.2010.02.077.
[38] M. Akhlaghi, S.A. Tayebifard, E. Salahi, M. Shahedi Asl, Spark plasma sintering of TiAl–Ti3AlC2 composite, Ceram. Int. 44 (2018) 21759–21764. https://doi.org/10.1016/j.ceramint.2018.08.272.
[39] M. Akhlaghi, E. Salahi, S.A. Tayebifard, G. Schmidt, Role of Ti3AlC2 MAX phase on characteristics of in-situ synthesized TiAl intermetallics. Part I: sintering and densification, Synth. Sinter. 1 (2021) 169–175. https://doi.org/10.53063/synsint.2021.1347.
[40] M. Akhlaghi, S.A. Tayebifard, E. Salahi, M. Shahedi Asl, G. Schmidt, Self-propagating high-temperature synthesis of Ti3AlC2 MAX phase from mechanically-activated Ti/Al/graphite powder mixture, Ceram. Int. 44 (2018) 9671–9678. https://doi.org/10.1016/j.ceramint.2018.02.195.
[41] T. Ai, F. Wang, X. Feng, M. Ruan, Microstructural and mechanical properties of dual Ti3AlC2–Ti2AlC reinforced TiAl composites fabricated by reaction hot pressing, Ceram. Int. 40 (2014) 9947–9953. https://doi.org/10.1016/j.ceramint.2014.02.092.